Potential energy landscape and long-time dynamics in a simple model glass

L. Angelani,[1] G. Parisi,[2] G. Ruocco,[3] and G. Viliani[1]
[1]*Universitá di Trento and Istituto Nazionale di Fisica della Materia, I-38050, Povo, Trento, Italy*
[2]*Universitá di Roma ''La Sapienza'' and Istituto Nazionale di Fisica Nucleare, I-00185, Roma, Italy*
[3]*Universitá di L'Aquila and Istituto Nazionale di Fisica della Materia, I-67100, L'Aquila, Italy*
(Received 7 April 1999; revised manuscript received 12 October 1999)

We analyze the properties of a Lennard-Jones system at the level of the potential energy landscape. After an exhaustive investigation of the topological features of the landscape of the systems, obtained by studying small size samples, we describe the dynamics of the systems in multidimensional configurational space by means of a simple model. This considers the configurational space as a connected network of minima where the dynamics proceeds by jumps described by an appropriate master equation. Using this model we are able to reproduce the long-time dynamics and the low temperature regime. We investigate both the equilibrium regime and the off-equilibrium one, finding those typical glassy behaviors usually observed in the experiments such as (i) a stretched exponential relaxation, (ii) a temperature-dependent stretching parameter, (iii) a breakdown of the Stokes-Einstein relation, and (iv) the appearance of a critical temperature below which one observes a deviation from the fluctuation-dissipation relation as a consequence of the lack of equilibrium in the system.

PACS number(s): 61.20.Lc, 64.70.Pf, 82.20.Wt

I. INTRODUCTION

The landscape paradigm [1] is a very useful point of view for the study of glassy systems. The detailed analysis of free energy or potential energy surfaces allows us to obtain insight into the rich phenomenology exhibited by glass-forming liquids in the supercooled phase, around the glass transition region and in the low temperature glassy regime. While the investigation of the free energy surface is a very hard task starting from a microscopic description of the system, since the landscape details are very strongly temperature dependent, the description of the potential energy landscape is a much more tractable problem, and is a good starting point to investigate properties at not-too-high temperatures. The trajectory of the representative point of the system in configurational phase space can be viewed as a path in the multidimensional potential energy surface. The dynamics is strongly influenced by the topography of the landscape: local minima, barrier heights, attraction basins, and further topological features. In recent years it has been shown that the details of the potential energy surface are of great importance in determining the properties of many systems exhibiting glassy behavior, like glass-forming liquids and protein folding, atomic cluster, or evolutionary biological models.

In this paper we numerically investigate the low temperature dynamical properties of a simple system, i.e. a monatomic Lennard-Jones system, through an analysis of its multidimensional potential energy surface and a simple model for the low temperature dynamics. In the first part (Sec. II), by studying a small sample size, we give a comprehensive description of the potential energy landscape of the systems—minima, barriers, reaction paths, and saddle points—and determine statistical distributions and cross-correlations between the analyzed quantities. In the second part (Sec. III), we use this information to set up a simple model for the study of the long-time relaxation dynamics of the system: The model consists of a connected network of potential energy minima with a jump dynamics described by an appropriate master equation. This allows us to obtain information about the behavior of the system for times long enough that a direct molecular dynamics (MD) simulation is not feasible [2]. After a static (thermodynamical) test of the model, we determine the dynamical equilibrium properties and also the off-equilibrium ones, and discuss the results. In Sec. IV we report the conclusions.

II. POTENTIAL ENERGY LANDSCAPE

We numerically investigate the topology of the potential energy hypersurface of a Lennard-Jones 6–12 system of N interacting particles in a cubic box with periodic boundary conditions. The pair potential is

$$V_{LJ}(r)=4\epsilon\left[\left(\frac{\sigma}{r}\right)^{12}-\left(\frac{\sigma}{r}\right)^{6}\right], \tag{1}$$

with r the Euclidean distance between two particles. The physical parameters σ and ϵ are chosen to describe an argon system: $\sigma=0.3405$ nm and $\epsilon/k_B=125.2$ K (k_B is the Boltzmann constant). In order to obtain an exhaustive description of the energy landscape, we investigate small size systems, with a number of particles $N<30$. As we shall see later, such small systems can nevertheless exhibit quite complex behaviors.

Due to the small size of the system, the range of interactions among the particles is of the same order as the box length. It is then much more appropriate to use a multi-image method instead of the usual minimum image method [3], in which each particle interacts only with the nearest image (generated by the periodic boundary conditions) of all other particles. In our case many images contribute, and it is necessary to consider them in the calculation of the interactions. The choice we made introduces an angular dependence in the pair potential which, however, is negligible with respect to the radial one. The simulated density is $\rho=4.2$

 ©2000 The American Physical Society

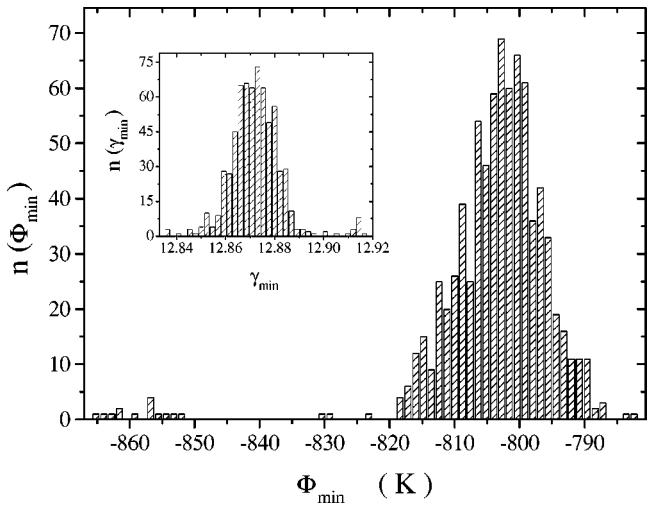

FIG. 1. Distribution of the potential energy (in K per particle) of the minima for the system $N=29$. In the inset the distribution of the curvature is γ_{min}.

$\times 10^{-2}$ mol/cm^3, which was obtained by Demichelis *et al.* [5] as the smallest value at which a Lennard-Jones system of $N=864$ argon particles is stable in the glassy state after a rapid quench from high temperature.

A. Minima

As a first step we search for the potential energy minima. We use a modified conjugate gradient method starting from high temperature configurations obtained during a MD simulation. In this way we find the so-called ''inherent configurations,'' corresponding to local minima. New minima are identified by their potential energy values. We analyze systems with $N=11$–29 and, for each N, we stop the search when the rate at which new low energy minima are found (for example in lowest first third of the full energy range) is smaller than a given number (about 10^{-4}). In this way we are able to obtain a good classification of the low energy minima. The number of detected minima, $\mathcal{N}$, does not show a clear and well defined dependence on N, contrary to the case of small clusters [6], so that it is not possible to give an estimate of the coefficient α in the expected exponential growth: $\mathcal{N}\propto\exp(\alpha N)$ (for clusters $\alpha\sim 1$). Indeed, for some values of N we observe a strong tendency of the system to fall always in the same minima. In this case an exhaustive research of the inherent structures is a very hard numerical task. This explains the unclear dependence found. Once most minima are classified, we analyze their features: energy, static structure factor, curvature, and distances.

1. Energy

The first important information about an inherent configuration is its potential energy value. From the energy distribution it is sometimes possible to recognize the crystallinelike configurations. Usually one finds an evident gap between the lowest energy minima, the crystallinelike ones, and the other ones with higher energies, as can be seen in Fig. 1 where we show the distribution of minima energies per particle for $N=29$. In other cases the situation is not so clear, and it is useful to use a different method to characterize the nature of an inherent configuration; the most useful quantity in determining the spatial order structure of a minimum is its static structure factor, which allows (imperfect) crystal-like configuration also of high energy to be identified.

2. Static structure factor

In order to classify the spatial distribution of particle in a given minimum of the potential energy we use the static structure factor

$$\hat{S}(\vec{q})=\frac{1}{N}\left|\sum_j \exp(i\vec{q}\cdot\vec{r}_j)\right|^2. \tag{2}$$

Due to the finite size of the system the allowed $\vec{q}$ vectors are of the form $\vec{q}=(2\pi/L)\ \vec{n}$, with $\vec{n}=(n_x,n_y,n_z)$ an integer vector. We define the quantity

$$S(q)=\frac{1}{n_q}\sum_{\vec{q}\in\{q,\Delta q\}}\hat{S}(\vec{q}), \tag{3}$$

where $\Sigma_{\vec{q}\in\{q,\Delta q\}}$ is a sum over the n_q vectors with modulus within $q\pm\Delta q$. For a pure crystalline configuration of N particles $S(q)$ consists of Bragg peaks, and its value at the peaks is $S_{max}=N$. For amorphous configurations $S(q)$ does not present a well defined peak structure, and the highest value is $S_{max}\sim 2$–3, obtained for a q value of the order of the inverse mean distance of two near particles. For small sized systems, like those analyzed here, there are intermediate situations and we use the criterion $S_{max}<N/2$ to determine the amorphous nature of an inherent structure.

3. Curvature

Another important property of a minimum is its overall curvature c, defined as the determinant of the Hessian Φ'' of the potential energy function Φ:

$$c=\det(\Phi''). \tag{4}$$

The eigenvalues of the Hessian matrix are proportional to the squared vibrational eigenfrequencies. In the inset of Fig. 1 we show the distribution of

$$\gamma=\frac{1}{3N-3}\log_{10}(c/m)^{1/2}, \tag{5}$$

where m is the mass of the particles (we use the argon value $m=40$ amu). The quantity γ is thus proportional to the sum of the logarithms of the frequencies of normal vibrational modes

$$\gamma=\frac{1}{3N-3}\sum_\alpha \ln\omega_\alpha, \tag{6}$$

with $\alpha=1,\ldots,3N-3$ (the three zero frequencies corresponding to rigid translations have been eliminated from the sum). As can be seen in Fig. 1, the highest γ values correspond to the minima with lowest energy, i.e. the crystallinelike minima which are narrower and deeper than the other packing structures (see also Sec. II C).

4. Stress tensor

For each minimum we determined the off-diagonal part of the microscopic stress tensor,

$$\sigma^{zx} = -\sum_{i<j} V'_{LJ}(r_{ij}) \frac{z_{ij}x_{ij}}{r_{ij}},$$

$$\sigma^{xy} = -\sum_{i<j} V'_{LJ}(r_{ij}) \frac{x_{ij}y_{ij}}{r_{ij}}, \tag{7}$$

$$\sigma^{yz} = -\sum_{i<j} V'_{LJ}(r_{ij}) \frac{y_{ij}z_{ij}}{r_{ij}},$$

where x_{ij}, y_{ij}, and z_{ij} are the components of $\vec{r}_{ij}=\vec{r}_i-\vec{r}_j$; these quantities will be useful in determining the shear viscosity. The form of the stress tensor we use is the $q=0$ extrapolation of the q-dependent expression [7]

$$\sigma_{\alpha,\beta}(\vec{q}) = \sum_i \left[m v_{i,\alpha} v_{i,\beta} - \sum_{i<j} \frac{r_{ij,\alpha} r_{ij,\beta}}{r_{ij}^2} P_q(r_{ij}) \right] \exp(i\vec{q}\cdot\vec{r}_i), \tag{8}$$

with

$$P_q(r) = r V'_{LJ}(r) \frac{1-\exp(i\vec{q}\cdot\vec{r})}{i\vec{q}\cdot\vec{r}}. \tag{9}$$

The indexes i and j refer to particles, while α and β label the spatial axes x, y, and z. In Eq. (7) we have omitted the kinetic term, not well defined in an inherent configuration; our hypothesis is that also this truncated form is well able to describe the relaxation processes.

5. Distances

We now turn to the relationships among the minima; in particular we determined the mutual distances in the $3N$-dimensional configuration space; in this regard it is important to take into account all the symmetry operations of the problem. Indicating with $\underline{r}_a=(\vec{r}_1^a, \ldots, \vec{r}_N^a)$ the $3N$ coordinates of the particles in the minimum a, we define the distances d_{ab} between minima a and b,

$$d_{ab} = \min_{T,R,\pi} (|\underline{r}_a - \underline{r}_b|), \tag{10}$$

where the minimization is made with respect to the continuous translations (T), discrete rotations and reflections (R), and permutations (π) of the particles.

The minimization over the continuous translations (T) is done by putting, sequentially, each particle of a in the same place as each one of b. The minimization over the rotations and reflections (R) is carried out by considering the 48 symmetry operations of the cubic group; the minimization over particle permutation (π) is apparently a hard task to solve, as one should consider all the $N!$ possible configurations in a direct calculation, but this is not actually the case. The problem is of polynomial type, i.e., the time needed to find the optimum solution grows as a polynomial function of the size, N, of the system (on the other hand nonpolynomial problems require an exponential computational time, i.e., the ''traveling salesman'' problem). The optimization problem we need to solve is a bipartite matching problem, which can be done in very short computational time by using an appropriate algorithm.

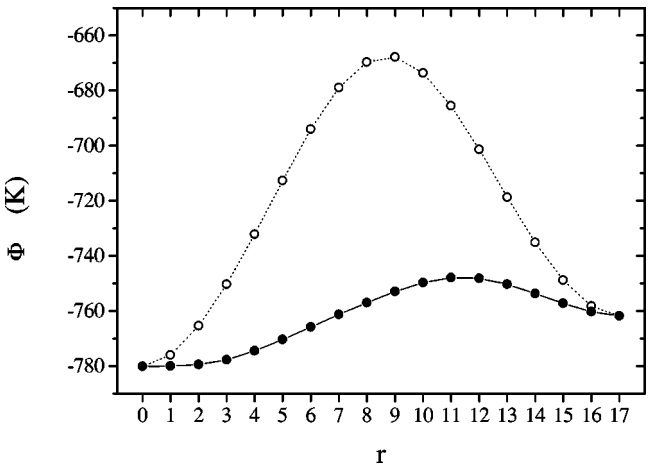

FIG. 2. An example of the potential energy profile along the least action path (●) between two minima, compared with the straight path (○) for the system $N=17$.

B. Barriers

A very important topological quantity in determining the dynamical behavior of the system is the energy barrier experienced by the system in traveling from one minimum to another. At first sight it might seem that it is accurate enough to evaluate the barrier along the straight path joining two minima in $3N$-dimensional space. However, as shown by Demichelis *et al.* [5], in most cases this produces much higher barriers than an evaluation along the least action path, indicating that the straight path approximation is often not good. We have then determined the least action path for each pair of minima a and b, which is defined as the path that minimizes the action functional

$$S[l] = \int_l ds \sqrt{2m[\Phi(\underline{r}(s)) - \Phi_0]}, \tag{11}$$

where l is a generic path between the minima, s is the curvilinear coordinate, and $\Phi_0=\min\{\Phi_a,\Phi_b\}$. This functional problem is simplified by dividing the path into a finite number of intervals (typically we use $n=16$ intervals) and by minimizing the action function with respect to the extreme of the n segments constrained to move in hyperplanes perpendicular to the straight path. The highest potential energy value along the least action path determines the barrier height and identifies the saddle point.

We have only analyzed the system with $N \leqslant 17$, due to the very long computational times needed in the cases with $N > 17$, where there are too many pairs of minima to take into account. We report the results for the largest system analyzed, $N=17$, with $\mathcal{N}=38$ minima. In Fig. 2 we show an example of the potential energy profile along the straight path (dashed line) and along the least action path (full line) between two minima. It is evident that the energy barrier is significantly lower in the latter case, although the two paths are not very distant in configuration space. Similar results are

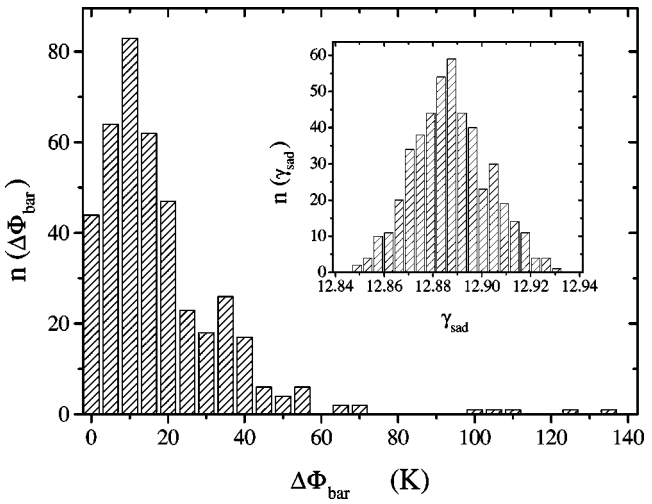

FIG. 3. Energy distribution of the barriers along the least action paths among the minima of the system $N=17$. The inset shows the distribution of the curvature γ_{sad} of the saddle points.

obtained for the other analyzed paths. Sometimes it happens that two minima are not directly connected, in the sense that the least action path joining them crosses a third minimum, and a nontrivial connectivity among the minima emerges (in the analyzed system we find that each minimum on an average is directly connected to 20 other minima). For each saddle point along the least action path we determine the main properties: energy, curvature, and down ''frequency.'' Figure 3 shows the energy distribution of the barriers $\Delta\Phi_{bar}$. The curvature is defined as the absolute value of the determinant of the Hessian of the potential energy evaluated at the saddle:

$$c_{sad}=|\det \Phi''_{sad}|. \tag{12}$$

In the inset of Fig. 3 we show the distribution of the quantity

$$\gamma_{sad}=\frac{1}{3N-3}\log_{10}(c_{sad}/m)^{1/2}. \tag{13}$$

The down ''frequency'' $\tilde{\omega}_{sad}$ is defined as the square root of the absolute value of the down curvature along the least action path,

$$\tilde{\omega}^2_{sad}=-\frac{\underline{v}\Phi''_{sad}\underline{v}}{|\underline{v}|^2}, \tag{14}$$

where $\underline{v}$ is the tangent vector to the least action path at the saddle point.

C. Correlations

In order to obtain a full statistical description of the potential energy landscape, it is also useful to investigate their cross-correlations, as well as the distributions of the different quantities. We then determined the linear correlation coefficient

TABLE I. Correlation coefficients r for the measured quantities x and y.

N	x	y	r
29	Φ_a	c_a	0.13
29	Φ_a	γ_a	0.46
29	$\lvert\Phi_a-\Phi_b\rvert$	d_{ab}	0.12
29	$\ln\lvert\Phi_a-\Phi_b\rvert$	$\ln d_{ab}$	0.17
17	$\lvert\Phi_a-\Phi_b\rvert$	d_{ab}	0.18
17	$\ln\lvert\Phi_a-\Phi_b\rvert$	$\ln d_{ab}$	-0.11
17	Φ_{sad}	c_{sad}	0.23
17	Φ_{sad}	γ_{sad}	0.49
17	c_{sad}	$\tilde{\omega}_{sad}$	-0.12
17	γ_{sad}	$\ln\tilde{\omega}_{sad}$	-0.31
17	d_{ab}	$\Delta\Phi_{bar}$	0.47
17	$\ln d_{ab}$	$\ln\Delta\Phi_{bar}$	0.67

$$r(x,y)=\frac{\sum_i (x_i-\overline{x})(y_i-\overline{y})}{\left[\sum_i (x_i-\overline{x})^2\sum_j (y_j-\overline{y})^2\right]^{1/2}} \tag{15}$$

for all the measured quantities x and y. Table I shows the values obtained, together with the log-log correlations, in order to highlight possible power laws. The first column gives the number of particles of the system analyzed (only for $N=17$ have we determined the least action paths and all the related quantities). Overall, it appears that the energy difference and distance among the minima are not correlated, indicating that the topological structure of the inherent configurations is not energy correlated. A weak correlation is observed between energy and curvature at stationary points (minima and saddle points). In Fig. 4 we show the cross-correlation between the energies of the minima and their curvatures. An interesting correlation is observed between barrier energies $\Delta\Phi_{bar}$ and distances among minima d_{ab} (Fig. 5), with a nearly linear correlation in double log scale (line in the figure).

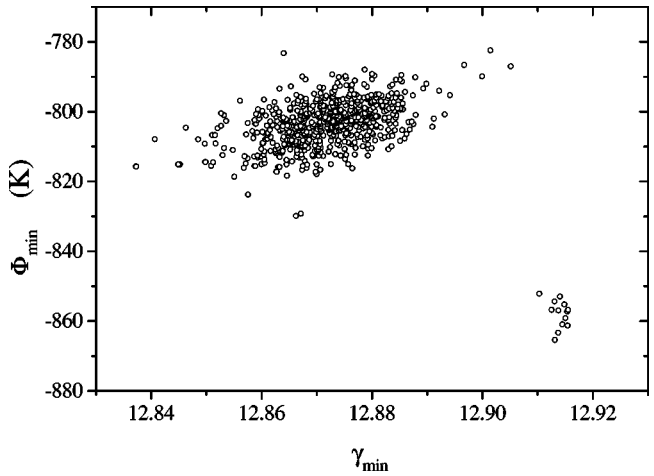

FIG. 4. Correlation between energies and curvatures of the minima ($N=29$). The highest curvature values correspond to low energy crystal minima.

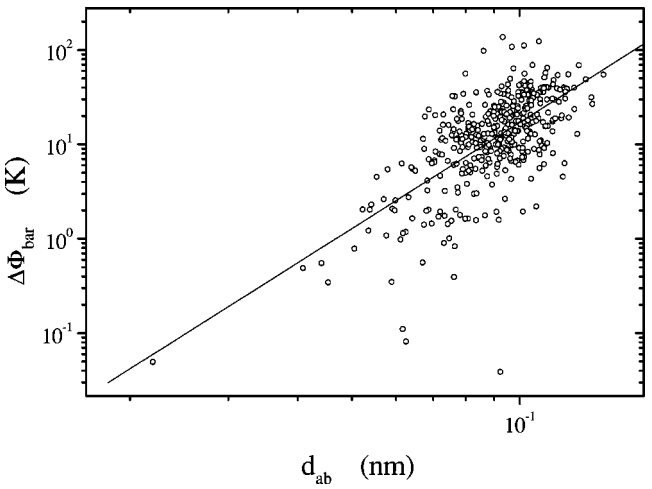

FIG. 5. Correlation between energies of the barriers and distances among minima, on a log scale ($N=17$). The line is the best linear fit on a log scale, corresponding to a power law fit (the slope is $\alpha=3.7$).

We conclude the analysis of the energy landscape by determining the entropy ratio R, defined as the ratio between the curvature of saddle points and that of the related minima

$$R=\frac{|\det \Phi''_{sad}|}{\det \Phi''_{min}}. \tag{16}$$

This quantity gives a quantitative measure of the ability of the system in finding the right path to reach another minimum. If $R\sim 1$, there are no entropic hindrances, while if $R \gg 1$ these effects become relevant, as the narrowness (higher value of the curvature) at the saddle makes the least action path toward that specific minimum unfavorable with respect to other escape routes. For all the minimum-saddle-minimum triplets we have evaluated R; the majority of the values is in the range 10^{-2}–10, in qualitative agreement with the results found in Lennard-Jones clusters [6].

III. MODEL FOR THE DYNAMICS

The investigation of the properties of glass-former liquids at the level of the energy landscape allows us to introduce some approximations in the dynamics of the system. We define a simplified model which is able to capture the long-time behavior of the system, and which consists of a connected network of potential energy minima with a jump dynamics among them described by an appropriate master equation [2].

The basic idea is quite simple. A glass structure is represented by a configurational point confined in a very small region of the accessible phase space and in the zero temperature limit (neglecting quantum effects), all the atoms are frozen in well-defined positions, corresponding to some mechanically metastable state. When the temperature is raised, jumps among different mechanically stable positions become possible. At finite and not-too-high temperatures we assume the dynamically relevant processes are the following: a short-time dynamics dominates by small vibrations around stable positions (this dynamics can be described within the harmonic approximation by diagonalizing the dynamical matrix), and a long-time dynamics consisting of collective jumps (involving many atoms) among different stable positions. The main hypothesis we make is that there is a substantially clear separation of time scales between the two dynamical processes. This characterization of the dynamics is a good approximation at not-too-high temperatures. By increasing the temperature, anharmonic effects become relevant to the vibration around the local minimum and, moreover, a clear time scale separation between fast vibrational and slow jumps dynamics is no longer possible. In a recent work [4] the validity of this hypothesis has been verified in Lennard-Jones binary mixtures with a direct MD investigation. To sum up, our model, which is expected to capture the physics of the system at low temperature, is based on two main hypotheses: (1) a clearcut difference between vibrational dynamics at short time and dynamics of collective jumps at long times; and (2) a description of the long-time dynamics through a master equation, with the transition rates that depend on the topological properties of the potential surface. The main advantages of the model we have described with respect to the usual MD computations are the following.

(a) In a simple way we can avoid the crystallization process that always takes place in one component LJ systems, as we do not consider the crystalline minima in setting up the network.

(b) We can study in a direct way the low temperature properties, where usually the very long relaxation times require very long computational time. In MD the computational times are proportional to the physical times, while in the model introduced here the computational times are those needed to find the eigenvalues and eigenvectors of the transition matrix, independent of temperature.

(c) It is possible to show the relationships between the energy landscape and the behavior of the system.

To be more specific, the model is a connected network of potential energy minima and the master equation governing the jumps dynamics is

$$\frac{dp_a}{dt}(t;b,t_0)=\sum_c W_{ac}p_c(t;b,t_0), \tag{17}$$

where $p_a(t;b,t_0)$ is the probability that the system is at minimum a at time t, if it was at minimum b at time t_0. The off-diagonal elements of the matrix W are the transition rates. The diagonal elements are fixed by the condition

$$\sum_a W_{ac}=0. \tag{18}$$

In order to obtain an asymptotic behavior that reproduces the right Boltzmann weight, the occupation probability must satisfy

$$\lim_{t\to\infty} p_a(t;b,t_0)=p_a^0\equiv\frac{1}{\mathcal{Z}}(\det \Phi''_a)^{-1/2}\exp(-\beta\Phi_a), \tag{19}$$

($\mathcal{Z}$ is such that $\Sigma_a p_a^0=1$, and the pre-exponential factor follows from the harmonic vibration in each minimum), and the transition matrix W must satisfy the detailed balance relation

$$W_{ab}p_b^0 = W_{ba}p_a^0. \tag{20}$$

The solution of the master equation is easily expressed in terms of eigenvalues λ_n and eigenvectors $\alpha_a^{(n)}$ ($n=1,\ldots,M$, with M the matrix dimension) of W:

$$p_a(t;b,t_0) = (p_b^0)^{-1}\sum_n \alpha_a^{(n)}\alpha_b^{(n)} \exp[\lambda_n(t-t_0)]. \tag{21}$$

In the numerical calculus it is more convenient to express the solutions in terms of the eigenvectors of a new symmetric matrix $w_{ab} = W_{ab}(p_b^0/p_a^0)^{1/2}$ (whose eigenvalues coincide with those of W):

$$p_a(t;b,t_0) = (p_a^0/p_b^0)^{1/2}\sum_n e_a^{(n)}e_b^{(n)} \exp[\lambda_n(t-t_0)]. \tag{22}$$

The model is well defined once we give an appropriate form to the transition matrix W. In order to determine the transition rates, let us analyze the problem of escape from a metastable state; a useful point of view for systems with many degrees of freedom is the description in terms of a few relevant coordinates. This reduction is possible whenever there are few reaction coordinates with characteristic evolutionary times longer than those of the other degrees of freedom, which act as effective terms on the relevant coordinates, i.e., like noise and viscous terms. We suppose this is the case for our system whenever the temperature is not too high (the analysis of reaction paths made by Demichelis *et al.* [5] supports this hypothesis). Handling the problem as a Markovian-Brownian d-dimensional motion in the overdamped friction regime, we obtain the form [8]

$$W_{ab} = \frac{\tilde{\omega}_{sad}^2}{\mu}\left[\frac{\det \Phi_b''}{|\det \Phi_{sad}''|}\right]^{1/2} \exp\left[-\frac{\Phi_{sad}-\Phi_b}{K_BT}\right], \tag{23}$$

where $\tilde{\omega}_{sad}$ is the down ''frequency'' at the saddle point, and μ is a friction constant that determines the time scale (its value is fixed by a comparison with MD in the allowed temperature region).

All the characteristics of the model (properties of the connected network and parameters in the transition rates) are inferred from the computed properties of the potential energy landscape. We use the values of the $N=29$ system to determine local minima properties (energy, curvature, and stress tensor), and those of the $N=17$ system to determine connectivity properties (energy and curvature of saddle points, distances, and connectivity among the minima). The values are extracted from the distribution found in Sec. II in the following ways.

(1) We extract M energy values of the minima from the distribution of $N=29$ system (we exclude the crystallinelike configurations).

(2) We assign to each minimum a value of curvature $c_a = \det \Phi_a''$ extracted from a bivariate distribution, thanks to the cross-correlation between energy and curvature; a stress tensor value is also extracted for each minimum.

(3) For each minimum we randomly extract (in the analysis of the energy landscape we have found no correlation between energies and distances among minima) 20 minima connected to it, as obtained on an average for the system $N=17$.

(4) We define a connection matrix κ_{ab}, containing the minimum steps, i.e., the number of minima crossed, necessary to go from a to b; the distance matrix d_{ab} is κ_{ab} times the value extracted from the distribution of the distances among connected minima for $N=17$.

(5) For each pair of directly connected minima we determine the energy barriers $\Delta\Phi_{bar}$ from the value of the distance d_{ab}: $\Delta\Phi_{bar} = A\ d^{\alpha}$ ($A \simeq 10^5$ and $\alpha \simeq 3.7$, as determined for $N=17$ system, Fig. 5).

(6) We assign a curvature value $c_{sad} = |\det \Phi_{sad}''|$ and a down ''frequency'' $\tilde{\omega}_{sad}$ to each saddle point, from bivariate distribution.

In this way we obtain a set of parameters that describes the model. In order to achieve a good statistical description, we considered different extractions of the parameters, and the measured quantities were obtained by averaging over the extractions.

A. Test

Before studying the dynamical properties of the model, we concentrate on the static behavior obtained as an asymptotic solution of the master equation. In this static regime we can determine, in a statistical mechanical approach, the configurational partition function

$$\mathcal{Z}(\beta) = \int d^{3N}r \exp[-\beta\Phi(\vec{r}_1,\ldots,\vec{r}_N)]. \tag{24}$$

By using the approximation based on the hypothesis of short-time local harmonic vibrations around a minimum, and long-time collective jumps among different minima, we obtain

$$\mathcal{Z}(\beta) \sim \sum_a \mathcal{Z}_a^{(harm)}(\beta)\exp[-\beta\Phi_a], \tag{25}$$

where a labels the minima, and $\mathcal{Z}_a^{(harm)}$ is the contribution of harmonic vibrations around minimum a. This form of the configurational partition function emerges in the model as the exact infinite-time limit. The harmonic term is easy to calculate, being a $3N$-dimensional Gaussian integral,

$$\mathcal{Z}_a^{(harm)}(\beta) = \int d\underline{r}\exp\left[-\frac{\beta}{2}\underline{r}\Phi_a''\underline{r}\right] = (2\pi)^{3N/2}\beta^{-3N/2}(\det \Phi_a'')^{-1/2}, \tag{26}$$

where $\underline{r} = (r_1,\ldots,r_{3N})$, and $\underline{r}\Phi_a''\underline{r} = \Sigma_{l,m} r_l(\Phi_a'')_{lm}r_m$. We then obtain the approximated partition function as

$$\mathcal{Z}(\beta) \sim c\beta^{-3N/2}\sum_a (\det \Phi_a'')^{-1/2}\exp(-\beta\Phi_a), \tag{27}$$

from which the thermodynamical quantities can be derived, for example for the energy $E(\beta) = -\partial_\beta \ln \mathcal{Z}$. To check the reliability of the model we compare the quantities calculated from Eq. (27) with those obtained through MD computation. In Fig. 6 we show the potential energy as obtained from the model (lines) and from MD (circles). The MD data are ob-

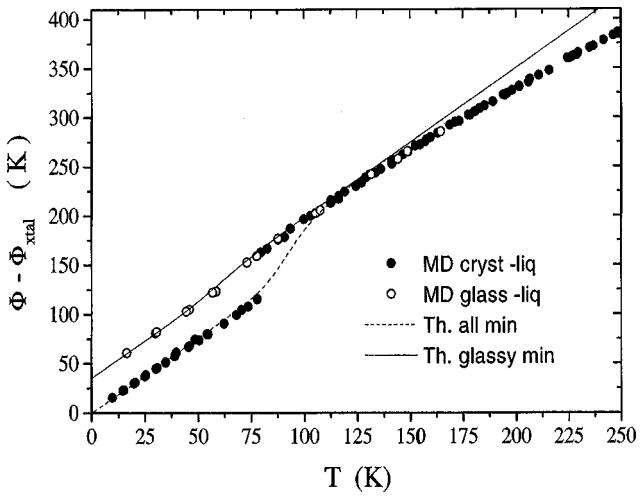

FIG. 6. Potential energy vs temperature as determined from MD ($N=29$) and from the model. The MD (○) are obtained by heating the glass and (●) cooling the liquid. The dotted line refers to the model using all the minima, and the full line to the model using only the glassy minima.

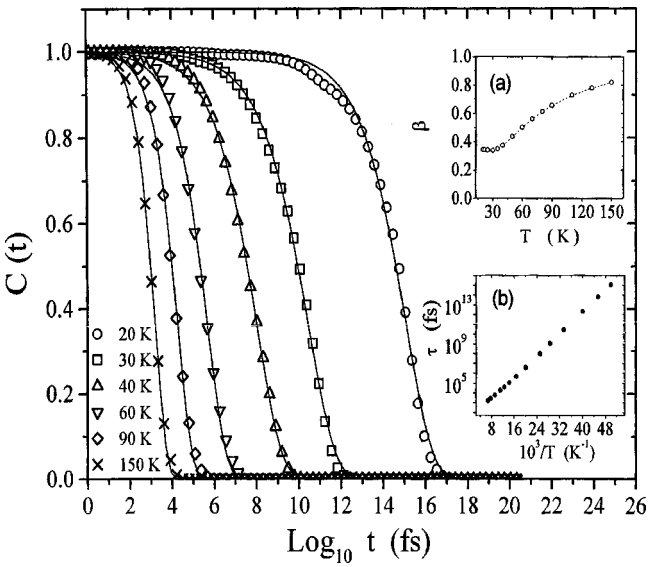

FIG. 7. Normalized autocorrelation functions of the off-diagonal microscopic stress tensor vs time at different temperatures, obtained from the model. In inset (a) we show the T dependence of the stretching parameter β_K, and in inset (b) the relaxation time vs $1/T$, both obtained from the stretched exponential fit of the autocorrelation functions.

tained in the following way. Starting from high temperature we rapidly quench the system to low temperature, entering in a glassy state; we then increase the temperature up to liquid phase (open circles). The system is subsequently slowly cooled, entering in the supercooled regime (100–70 K) and at the end obtaining the crystal through a first order transition (full circles). The lines represent the energies determined from the model by taking into account all the minima (dotted line) and only the glassy ones (full line). A good quantitative agreement is obtained between MD and the model as far as the temperature is lower than about 150 K, a temperature in the liquid phase well above the melting point ($T_m \sim 80$ K). This result supports the correctness of the approximation of local vibration and collective jumps in the description of a glass former at not-too-high temperature. This static test is a good starting point to extend the analysis to the dynamical regime.

B. Equilibrium properties

We now determine the dynamical equilibrium properties of the model. With $O(r(t),r(0))$ we denote a generic observable which depends on collective coordinates r at time t and at initial time $t=0$. We define the statistical average value of O in the model as

$$\langle O(t)\rangle = \sum_b p_b^0 \sum_a O_{ab} p_a(t;b,0), \tag{28}$$

where O_{ab} is the value of O evaluated at the minimum configurations a and b: $O_{ab}=O(r_a,r_b)$. In terms of the eigenvalues and eigenvectors of the transition matrix W, we have

$$\langle O(t)\rangle = \sum_n \exp(\lambda_n t) \sum_{a,b} O_{ab} \alpha_a^{(n)} \alpha_b^{(n)}, \tag{29}$$

or, in terms of the eigenvectors of the symmetric matrix w,

$$\langle O(t)\rangle = \sum_n \exp(\lambda_n t) \sum_{a,b} O_{ab} (p_a^0 p_b^0)^{1/2} e_a^{(n)} e_b^{(n)}. \tag{30}$$

In the following we report a detailed analysis of the equilibrium dynamics for a network of 400 minima, averaging over 50 different extractions of the parameters that define the model. We measure the time autocorrelation function of the stress tensor, the shear viscosity, the structural relaxation times, and the mass diffusion coefficient.

We first determine the time autocorrelation functions of a structural quantity which is well defined in all minimum configurations, i.e., the off-diagonal microscopic stress tensor (7). The correlation function is

$$C(t) = \frac{1}{3}[\langle \sigma^{zx}(t)\sigma^{zx}(0)\rangle + \langle T^{xy}(t)T^{xy}(0)\rangle + \langle T^{yz}(t)T^{yz}(0)\rangle]. \tag{31}$$

The quantity O_{ab} in Eq. (22) is, in this case,

$$O_{ab} = \frac{1}{3}[\langle \sigma_a^{zx}\sigma_b^{zx}\rangle + \langle T_a^{xy}T_b^{xy}\rangle + \langle T_a^{yz}T_b^{yz}\rangle]. \tag{32}$$

We have measured the correlation functions for different temperatures, from $T=150$ to 20 K. In Fig. 7 we report the normalized correlation functions $C(t)/C(0)$ at different temperatures (open symbols) together with the best stretched exponential fit (lines):

$$C(t) = C(0)\exp[-(t/\tau)^{\beta_k}]. \tag{33}$$

Contrary to the MD computations, which result in a two-steps behavior for the relaxation processes (one associated with fast local dynamics and the other with structural slow dynamics, the so-called α structural processes), the model gives only one relaxation step, associated with the structural processes, because the model can only describe the long-time

behavior. The results we obtain with the present model are consistent with those of MD in the allowed region (i.e., above $T\sim 90$ K, in order to avoid crystallization in the MD computation). In inset (a) we show the temperature dependence of the stretching parameter β_k. It emerges that the structural relaxation dynamics is well represented by a stretched exponential decay, and that the stretching parameter β_k is strongly temperature dependent.

Both results are well supported by experimental [9] and numerical [10] observations. In our case the stretching parameter β_k decreases from a value of ~ 1 at high temperature to $\beta_k \sim 0.35$ at low temperature, in agreement with experimental findings [9].

From the behavior of the correlation function $C(t)$ we can obtain information about the structural relaxation time τ. The values of τ [inset (b)] are determined from the stretched exponential fits. We obtain an increase of many orders of magnitude in a small temperature range, as usually found in many glass-forming liquids. However, we do not find the dramatic increase of the Vogel-Tammann-Fulcher type expected for a fragile glass former [11]. It is possible that the observed Arrhenius behavior emerges as a peculiar property of the model, which would mean that the model is unable to capture the phenomenology of ''fragility.'' It is, however, possible that the Arrhenius law is a genuine property of glass-forming liquids with Lennard-Jones interaction, as supported by a comparison with a MD computation in the allowed temperature range. It would be very interesting to compare the behavior obtained from the model to the ''true'' behavior (in the sense of MD computation) in the full temperature range (this is possible only for those systems that avoid crystallization, like suitable binary mixtures).

Finite size effects can also be responsible for the observed Arrhenius behavior. The small size sample implies an upper bound to the energy barrier for the global rearrangement and then an Arrhenius upper bound to the relaxation time, $\tau \leqslant \tau_o \exp \beta N a$, with τ_o a system dependent constant. The finite size study needed to verify the latter possibility is a very hard task, the number of minima growing exponentially with the number of particles. So we are not able to investigate more accurately the size effects and the reliability of the Arrhenius behavior is still an open question.

From the time autocorrelation functions of the off-diagonal microscopic stress tensor, we can determine the shear viscosity as [7]

$$\eta = \frac{1}{k_B T V} \int_0^\infty dt\ C(t). \tag{34}$$

Also in this case, as for the relaxation times, we find a strong increase in a small temperature range, from $\eta \sim 10^{-2}$ P at $T=150$ K, to $\eta \sim 10^{11}$ P at $T=20$ K. Again, we found there was close correspondence between the model and MD for $T>90$ K, giving further support to the model.

The last quantity we measured in the model was the mass diffusion coefficient. In order to find it we determine the mean square displacement

$$O(t) = \frac{1}{N} |\underline{r}(t) - \underline{r}(0)|^2 = \frac{1}{N} \sum_{i=1}^{N} |\vec{r}_i(t) - \vec{r}_i(0)|^2, \tag{35}$$

from which we obtain the diffusion coefficient

$$D = \lim_{t\to\infty} \frac{O(t)}{6t}. \tag{36}$$

To evaluate D we use the quantity $O_{ab} = d_{ab}^2/N$, where d_{ab} was defined in Eq. (10). We again observe a strong increase with an interesting behavior not simply linear on a double logarithmic scale [2].

We conclude this section by analyzing the validity of the Stokes-Einstein relation in the model. The Stokes-Einstein relation describes in a rigorous way the diffusive motion of a macroscopic object in a fluid, and predicts the following relation:

$$D \propto \frac{T}{\eta}. \tag{37}$$

The Stokes-Einstein relation also describes fairly well the diffusion at atomic scale in liquids at high temperatures. By lowering temperature, as observed in many experiments [12], one usually finds a breakdown of Eq. (37). We found [2] that at high T the model asymptotically satisfies the Stokes-Einstein relation, but upon decreasing T we observe a breakdown of the relation and a fit over the lowest temperature data of the type

$$D^{-1} \propto \left(\frac{\eta}{T} \right)^{\xi} \tag{38}$$

that gives the value

$$\xi \simeq 0.28. \tag{39}$$

This value is in fairly good agreement with experimental results found in fragile glass formers, like o-terphenyl [13].

C. Off-equilibrium properties

Although introduced to analyze the long-time dynamics, the model allows an easy computation of the short-time, off-equilibrium dynamics. One of the main properties of glass formers is the very strong increase of characteristic relaxation times when temperature is lowered. If these times become comparable to observational times, the system is no longer able to explore the full accessible phase space and then to reach the thermal equilibrium. The observed quantities are characterized by off-equilibrium processes. In this regime the one-time quantities, such as energy or time correlation functions with fixed initial time, can no longer describe the physics of the system. The usual translational time invariance, valid in the equilibrium regime, is no more satisfied. One of the most interesting consequences of that is the fact that the fluctuation-dissipation relation no longer holds [14]. We concentrate on this property here.

Let H be the Hamiltonian of the system, and O a generic observable dependent on microscopic variables. We define the two time autocorrelation function

$$C(t,t_w) = \langle O(t) O(t_w) \rangle, \tag{40}$$

where we suppose that $t>t_w$, and $\langle \cdots \rangle$ now means a dynamical average over initial conditions. We also introduce

the response function to a perturbation ϵ, which is coupled to the observable O and gives rise to a perturbed Hamiltonian:

$$H' = H + \epsilon(t)O, \tag{41}$$

The response is defined as

$$R(t,t_w) = \left.\frac{\delta\langle O(t)\rangle}{\delta\epsilon(t_w)}\right|_{\epsilon=0}, \tag{42}$$

where again $t > t_w$. In the equilibrium regime the time translational invariance implies the validity of fluctuation dissipation relation [15]

$$R_{eq}(\tau) = \beta\frac{\partial C_{eq}(\tau)}{\partial\tau}, \tag{43}$$

where $\tau = t - t_w$. Introducing the integrate response function χ,

$$\chi(t,t_w) = \int_{t_w}^{t} dt' R(t,t'), \tag{44}$$

Eq. (43) takes the form

$$\frac{d\chi(C)}{dC} = \beta. \tag{45}$$

In the off-equilibrium regime the fluctuation-dissipation ratio (45) is no longer valid. It is possible, however, to generalize the ratio introducing a violation factor $X(t,t_w)$. The analytical study of some generalized mean field spin glass models [16] shows that the function $X(t,t_w)$ depends on time only through the correlation function C: $X(t,t_w) = X[C(t,t_w)]$. Using this property we can write a generalized fluctuation-dissipation ratio in the off-equilibrium regime

$$\frac{d\chi(C)}{dC} = \beta X(C). \tag{46}$$

For short times $\tau \ll t_w$ we have $X(C) = 1$, and the system satisfies an equilibriumlike relation, even if it is confined in a small phase space region. For times $\tau \sim t_w$ the exploration of the phase space is an off-equilibrium process, and this implies the violation of the equilibrium fluctuation-dissipation ratio. In this case we have $X(C) < 1$. The very interesting relationship between off-equilibrium and equilibrium properties of some generalized spin glass model suggests that, in the case of one step replica symmetry breaking, the $X(C)$ function depends only on temperature,

$$X(C) = m(T), \tag{47}$$

and $m(T)$ is linear in T at low temperature. It was recently suggested that structural glasses present a striking similarity with the generalized spin glass model with one step replica symmetry breaking [17] (for a recent interesting review, see Coluzzi [19]). We then also expect that for structural glasses the violation parameter would show a linear temperature dependence in the violation region $X < 1$. Evidence of this behavior was found in a recent numerical study of binary mixtures [18]; we analyze this in our model.

Let $O(r(t))$ be a generic observable that depends on collective coordinates at time t. The average value of O in the off-equilibrium regime in the model is

$$\langle O(t)\rangle = \frac{1}{M'}\sum_{a,b} O_a p_a(t;b,0), \tag{48}$$

where a and b label the minima, and the sum over b is now limited to a certain subset of minima. We chose the M' highest energy states. Expression (48) differs from the equilibrium one, as the initial states are weighted with a constant term (corresponding to an infinite temperature) rather than with the Gibbs-Boltzmann equilibrium weight. In this way we describe an instantaneous quench at time $t = 0$ from $T = \infty$ to a finite temperature T (the T dependence is as usual in the probability p_a). The sum restricted to the M' initial states with highest energies ($M' < M$ where M is the total number of minima; in our case $M = 400$ and $M' = 20$) allows a better description of the off-equilibrium regime. We calculate the time correlation functions in the model as

$$\langle O(t)O(t_w)\rangle = \frac{1}{M'}\sum_{a,b,c} O_a O_b p_b(t_w;c,0)p_a(t;b,t_w), \tag{49}$$

where the sum over b is still made over the M' highest minima. The quantity we determine is the time autocorrelation function of the off-diagonal microscopic stress tensor σ^{zx}:

$$C(t,t_w) = \langle\sigma^{zx}(t)\sigma^{zx}(t_w)\rangle - \langle\sigma^{zx}(t)\rangle\langle\sigma^{zx}(t_w)\rangle. \tag{50}$$

The response function is determined by the perturbed Hamiltonian

$$H' = H + \epsilon(t)\sigma^{zx}, \tag{51}$$

where the external field ϵ is

$$\epsilon(t) = \begin{cases} 0 & \text{for } t < t_w \\ \epsilon & \text{for } t \geq t_w. \end{cases} \tag{52}$$

The perturbation induces a change in the energies of the minima:

$$\Phi_a' = \Phi_a + \epsilon(t)\sigma_a^{zx}. \tag{53}$$

The response function is

$$R(t,t_w) = \left.\frac{\delta\langle\sigma^{zx}(t)\rangle_\epsilon}{\delta\epsilon(t_w)}\right|_{\epsilon=0}. \tag{54}$$

$\langle\cdots\rangle$ is evaluated in the presence of the perturbation ϵ,

$$\langle\sigma^{zx}(t)\rangle_\epsilon = \frac{1}{M'}\sum_{a,b,c}\sigma_a^{zx} p_b(t_w;c,0)p_a^\epsilon(t;b,t_w), \tag{55}$$

where p^ϵ is the solution of the master equation with the perturbing term. For small perturbations we obtain

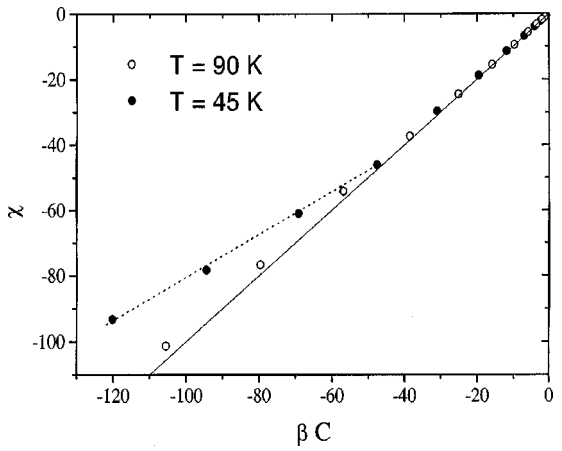

FIG. 8. The integrate response χ vs βC at temperatures $T=90$ K (○) and $T=45$ K (●). The value of the waiting time is $t_w=300$ fs. The full line is the fluctuation-dissipation ratio, and the dotted line is the best fit of the last points of $T=45$ K.

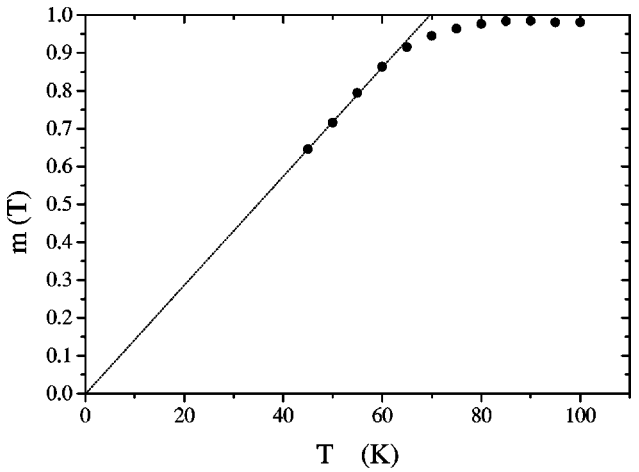

FIG. 9. The slope m in the region of violation of the fluctuation-dissipation ratio vs temperature. The straight line fits the data in the violation region.

$$\chi(t,t_w)=\frac{\langle\sigma^{zx}(t)\rangle_\epsilon-\langle\sigma^{zx}(t)\rangle_{\epsilon=0}}{\epsilon}. \tag{56}$$

We have determined the correlation functions $C(t,t_w)$ and the response $\chi(t,t_w)$ as functions of t for different times t_w; the temperatures we analyze are in the range $T=100$–20 K. The t_w values are chosen in such a way that $t_w \ll \tau(T)$ for all temperatures T analyzed (τ is now the relaxation time). We note that in the case $t_w \gg \tau$ the fluctuation-dissipation theorem is recovered, the average over initial conditions now being over an equilibrium ensemble, with a Gibbs-Boltzmann weight $\exp-\beta\Phi_a$. The dynamical processes analyzed here are then in a time range which is very small compared to the time scale of the equilibrium. In determining the response functions we have used a value of ϵ small enough ($\epsilon=0.1$) to make the regime linear, as verified by trying different ϵ values. In Fig. 8 we report the behavior of χ versus βC at temperatures $T=90$ and 45 K, respectively. While at $T=90$ K the relation between χ and βC is to a good approximation linear with slope 1 on the whole range (full line), at lower temperature it is evident that after a first linear behavior with slope 1 (full line) an approximately linear behavior with slope <1 takes on at longer times (dashed line), as theoretically and numerically expected. The C values are not numerically comparable to the C equilibrium values of Fig. 7, because we have used a more suitable form of the correlation. They correspond to the small time scale values of the equilibrium behavior.

Moreover the slope of the second region decreases by lowering temperature: in Fig. 9 we show the slope m of the violation region versus T. At high temperature the value of m is nearly 1, while below a temperature of about 60–70 K, m decreases linearly, as we expect in the hypothesis of one-step replica symmetry breaking. Figure 9 is limited to $T>40$ K, as for lower temperatures the m values saturate to a limiting value and it is no longer possible to extract correct information. This effect is probably due to the finite size of the system, because the sampling of the initial off-equilibrium states is not exhaustive ($M'=20$). In the equilibrium analysis the finite size effects do not show up in the temperature range explored, as the sampling of the initial states is complete ($M'=M$). In conclusion, from an analysis of the off-equilibrium properties of the model, it emerges that the deviation from the usual fluctuation-dissipation relation, valid in the equilibrium regime, is in agreement with theoretical predictions and numerical findings in simple glass formers.

IV. CONCLUSIONS

The very rich phenomenology of the cooling process of glass-forming liquids, of the glass transition, and of glassy systems in general, has received many important theoretical, numerical, and experimental contributions in the last few years. The present work is concerned with a numerical investigation of a simple model glass: a Lennard-Jones system of interacting particles. The main aim of the work was to determine the emergent properties of the system at the level of the potential energy landscape. After a detailed analysis of the topological properties of the potential energy surface, we introduced a model which reproduces the long-time dynamic behavior of the system. While in the usual MD investigations of relaxation the computational times are proportional to physical times (with computational times of the order 10^5 s, one obtains physical times of the order 10^{-9} s for a system of size $N\sim10^3$), our model allows the study at very long physical times in short computational times.

We studied both equilibrium and off-equilibrium properties. The main equilibrium results we obtained are (i) the stretching of the relaxation dynamics, (ii) the temperature dependence of the stretching parameter, and (iii) the breakdown of the Stokes-Einstein relation. If they are genuine properties of the glassy system analyzed, they represent intriguing and interesting results that open fascinating questions about the behavior of glassy and supercooled liquids.

Although introduced to investigate the long-time dynamics, the model is also able to describe the off equilibrium dynamics in a simple and direct way. The emergent violation of the fluctuation-dissipation relation (that holds at equilibrium) is a very interesting feature, and supports many conjectures about the analogy between structural glasses and some spin glass models [17]. Moreover, the appearance of a

critical temperature, below which the violation takes place, seems to indicate the existence of a transition; the ''inconsistency'' with the Arrhenius behavior of the relaxation time at equilibrium is an open question and deserves further studies (finite size effects and reliability of the ''rate equation'' dynamics).

In conclusion, the analyzed features of the potential energy landscape, and the emergent properties of the model both at and off equilibrium, seem to provide a good description of glassy systems. The method is very powerful for the investigation of glassy properties by avoiding some of the main problems usually encountered in numerical studies, like the very long computational times in the low temperature regime or the presence of crystal states. We hope the analysis we performed may constitute a promising route in the investigation of glassy systems.

ACKNOWLEDGMENTS

We acknowledge B. Coluzzi, G. Monaco, F. Sciortino, and P. Verrocchio for useful discussions, and D. Leporini who kept our attention on the fractional SE relation issue.

[1] M. Goldstein, J. Chem. Phys. **51**, 3728 (1969); G. Adam and J. H. Gibbs, *ibid.* **57**, 470 (1972); F. H. Stillinger and T. A. Weber, Phys. Rev. A **28**, 2408 (1983); F. H. Stillinger, Science **267**, 1935 (1995); J. P. K. Doye and D. J. Wales, J. Chem. Phys. **105**, 8428 (1996); C. A. Angell, Nature (London) **393**, 521 (1998); S. Sastry, P. G. Debenedetti, and F. H. Stillinger, *ibid.* **393**, 554 (1998).

[2] L. Angelani, G. Parisi, G. Ruocco, and G. Viliani, Phys. Rev. Lett. **81**, 4648 (1998).

[3] M. P. Allen and D. J. Tildesley, *Computer Simulation of Liquids* (Oxford University Press, Oxford, 1987).

[4] T. B. Schroder, S. Sastry, J. C. Dyre, and S. C. Glotzer, e-print cond-mat/9901271.

[5] F. Demichelis, G. Viliani, and G. Ruocco, Phys. Chem. Commun. 005 (1999).

[6] G. Daldoss, O. Pilla, and G. Viliani, Philos. Mag. B **77**, 693 (1998); G. Daldoss, O. Pilla, G. Viliani, C. Brangian, and G. Ruocco, Phys. Rev. B **60**, 3200 (1999).

[7] U. Balucani and M. Zoppi, *Dynamics of the Liquid State* (Oxford University Press, Oxford, 1994).

[8] H. Risken, *The Fokker-Planck Equation* (Springer-Verlag, Berlin, 1984); P. Hanggi, J. Stat. Phys. **42**, 105 (1985).

[9] M. T. Cicerone, F. R. Blackburn, and M. D. Ediger, J. Chem. Phys. **102**, 471 (1995).

[10] S. Sastry, P. G. Debenedetti, and F. H. Stillinger, Nature (London) **393**, 554 (1998); W. Kob and H. C. Andersen, Phys. Rev. E **52**, 4134 (1995).

[11] C. A. Angell, Science **267**, 1924 (1995).

[12] R. Kind, O. Liechti, N. Korner, J. Hulliger, J. Dolinsek, and R. Blinc, Phys. Rev. B **45**, 7697 (1992); F. Fujara, B. Geil, H. Sillescu, and G. Fleischer, Z. Phys. B: Condens. Matter **88**, 195 (1992); I. Chang, F. Fujara, B. Geil, G. Heuberger, T. Mangel, and H. Sillescu, J. Non-Cryst. Solids **172-174**, 248 (1994); F. R. Blackburn, M. T. Cicerone, G. Heitpas, P. A. Wagner, and M. D. Ediger, *ibid.* **172-174**, 256 (1994).

[13] L. Andreozzi, A. Di Schino, M. Giordano, and D. Leporini, J. Phys.: Condens. Matter **8**, 9605 (1996).

[14] J. P. Bouchaud, L. F. Cugliandolo, J. Kurchan, and M. Mezard, in *Spin Glasses and Random Fields*, edited by P. Young (World Scientific, Singapore, 1997); e-print cond-mat/9702070.

[15] G. Parisi, *Statistical Field Theory* (Addison-Wesley, New York, 1988).

[16] L. F. Cugliandolo and J. Kurchan, Phys. Rev. Lett. **71**, 173 (1993); Philos. Mag. B **71**, 501 (1995); J. Phys. A **27**, 5749 (1994).

[17] T. R. Kirkpatrick and P. G. Wolynes, Phys. Rev. B **35**, 3072 (1987); T. R. Kirkpatrick and D. Thirumalai, *ibid.* **36**, 5388 (1987); L. Cugliandolo and J. Kurchan, Phys. Rev. Lett. **71**, 173 (1993); S. Franz and G. Parisi, *ibid.* **79**, 2486 (1997); G. Parisi, e-print cond-mat/9712079; e-print cond-mat/9701034; B. Coluzzi and G. Parisi, e-print cond-mat/9712261.

[18] G. Parisi, Phys. Rev. Lett. **79**, 3660 (1997); J. L. Barrat and W. Kob, Europhys. Lett. **46**, 637 (1999).

[19] B. Coluzzi, Ph.D. thesis, Universitá di Roma ''La Sapienza,'' 1998 (unpublished).